Self-energy calculations in the Hubbard model

1993 J. Phys.: Condens. Matter 5 5649

(http://iopscience.iop.org/0953-8984/5/31/026)

J. Phys.: Condens. Matter 5 (1993) 5649–5662. Printed in the UK

Self-energy calculations in the Hubbard model

C J Rhodes and R L Jacobs

Department of Mathematics, Imperial College of Science, Technology and Medicine, 180 Queen's Gate, London SW7 2BZ, UK

Received 27 July 1992, in final form 8 April 1993

Abstract. We have calculated the electronic self-energy of the two-dimensional Hubbard model as a function of frequency *and* momentum for various band fillings. We present this up to second order in the interaction parameter and also up to infinite order for ladder diagrams in the two-particle scattering channel. We have carried out direct k-space integrations using a triangle method. For a half-filled perfectly nested band, the imaginary part, $\mathrm{Im}\,\Sigma(k_f, \omega)$, has a linear-$\omega$ dependence for nested Fermi surfaces which is consistent with the marginal Fermi liquid phenomenology for high-T_c superconductors. At, and near, half-filling there is a strong low-energy peak in $\mathrm{Im}\,\Sigma^{(2)}(k, \omega)$ when k is off the Fermi surface. The physical origin of this peak will be discussed. The peak is enhanced in the ladder approximation. The corresponding structure in $\mathrm{Re}\,\Sigma^{(2)}(k, \omega)$ leads to multiple solutions of the Dyson equation for a wide range of values of the parameters. This leads to an appealing explanation of observed structure in some experimental angle-resolved photoemission spectra of high-T_c materials. We also find anti-bound states split off from the band in the two-particle scattering ladders consistent with the suggestion of Anderson.

1. Introduction

The Hubbard model is a subject of perennial interest to theoretical physicists. Recently much work has been done using the two-dimensional Hubbard model as a description of the properties of high-temperature superconductors. Despite its apparent simplicity there are many difficulties in extracting useful results. Attempts at a purely analytic solution quickly run into intractable difficulties. The only exact results that exist for the Hubbard model are in one dimension [1], though there are great simplifications in infinite dimensions [2]. Another approach is to use quantum Monte Carlo simulations or similar numerical techniques [3]. There are difficulties associated with this approach also because rather small cluster sizes have to be used to obtain a result in a realistic amount of computer time. In view of this, *any* results concerning the two- and three-dimensional cases are of interest.

Apart from their high transition temperatures, high-T_c materials exhibit unusual normal-state properties, some of which cannot be understood in terms of a conventional Fermi liquid interpretation. This has led to speculation that the electronic ground state in these systems is not a Fermi liquid. If this is the case then it would invalidate conventional theoretical approaches to the superconducting state which assume pairing of opposite-spin quasiparticles in a Fermi liquid background. There have been many different non-Fermi liquid theories proposed [4]. Some believe that the essential feature of these materials is strong electron correlation. This has been developed by Anderson in the RVB theory [5] to account for normal-state properties and the superconducting state. Various phenomenologies of the normal state have also been put forward to address either individual experiments or a broad class of results. The marginal Fermi liquid phenomenological hypothesis of Varma

0953-8984/93/315649+14$07.50

and co-workers [6] has been successful in accounting for several different experiments and implies a non-Fermi liquid ground state. A proposed justification of the marginal Fermi liquid phenomenology has been provided in the nested Fermi liquid theory of Virosztek and Ruvalds [7] in which they derive equations for the susceptibility with the same functional form. The nested Fermi liquid theory is based on a weak-coupling treatment of the two-dimensional Hubbard model.

Our approach is firstly to calculate $\Sigma(k,\omega)$ in second-order perturbation theory as accurately as possible using a direct k-space integration by a triangle method [8] and secondly to carry out the obvious extension to higher-order perturbation theory by summing ladder diagrams in the two-particle scattering channels. Our careful numerical calculation demonstrates that there are new and unexpected structures in the self-energy which are robust to simple higher-order perturbative corrections. The consequences of these new effects should be taken into account in any more sophisticated many-body theory of the Hubbard model.

The low-order results we obtain confirm the nested Fermi liquid results of Virosztek and Ruvalds. The results also display other interesting behaviour at rather low values of ω. The imaginary part of the self-energy has a strong low-ω peak, which develops as k moves off the Fermi surface; this peak has a nearly discontinuous upper edge. The peak persists and is, indeed, enhanced in the ladder approximation. In view of the possible physical importance of this new feature we have devoted some effort at understanding its origin. The peak is also present in the one-dimensional results where it can be understood more easily. It arises from the fact that the energy denominator in $\Sigma^{(2)}(k,\omega)$ has two distinct maxima in widely separated nearly discrete regions of phase-space corresponding to forward and backward scattering across the Fermi surface. The peak in the low-energy imaginary part of the self-energy implies a corresponding feature in the real part and has consequences for the spectral density and for the calculation of the ARPES spectrum. Some experimental ARPES results display similar structures which can be explained in terms of our results.

In section 2 we describe the triangle method used to calculate the self-energies and in section 3 discuss the results for the half-filled case. The interesting new peaked feature at low energies and its physical consequences in the calculation of ARPES results are analysed in section 4 in terms of the contributions to the total self-energy from individual q-summations.

In section 5 we present the self-energy calculations for non-nested Fermi surfaces. These include a doped bandstructure with nearest-neighbour hopping and a bandstructure that introduces next-nearest-neighbour hopping. Section 6 describes the calculation and results for the infinite-order scattering diagram and its relation to the ideas of Anderson concerning the splitting off of higher-energy bound states from the band.

2. Method of calculation

We start with the two-dimensional Hubbard model

$$H = -t\sum_{i,j,\sigma}(c^{+}_{i\sigma}c_{j\sigma} + \text{HC}) + U\sum_{i}(n_{i\uparrow}n_{i\downarrow}) \tag{1}$$

where U is the on-site Coulomb repulsion and t is the hopping integral.

It is possible to examine this Hamiltonian in a variety of limits depending on the strength of the correlation. We shall first calculate the second-order self-energy correction, $\Sigma^{(2)}(k,\omega)$, defined by the diagram in figure 1:

$$\Sigma^{(2)}(k,\omega) = \frac{U^2}{(2\pi)^4}\int\int \frac{f_p(1-f_{p-q})(1-f_{k+q})}{\omega+\varepsilon_p-\varepsilon_{k+q}-\varepsilon_{p-q}-\mathrm{i}\delta}\mathrm{d}^2q\,\mathrm{d}^2p \;+\; \text{a similar term for holes.} \tag{2}$$

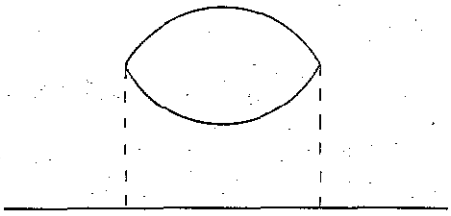

Figure 1. Bubble diagram for second-order perturbation calculation of $\Sigma^{(2)}(k, \omega)$.

Using a direct numerical integration technique we are able to calculate the frequency- and momentum-dependence of the imaginary part of the self-energy for the two-dimensional Hubbard model for various bandstructures and bandfillings. The real parts are obtained by a Hilbert transform of the imaginary parts. The results are of relevance to the conclusions of the nested Fermi liquid theory, which may provide a microscopic justification of the marginal Fermi liquid hypothesis of Varma and co-workers [6].

To evaluate the momentum integrals in (2) we use a triangle method which is an adaptation to two dimensions of the tetrahedron method [8].

We first calculate the imaginary part of the q integral in the particle–particle channel:

$$\Pi^{(p)}(k, p, \omega + \varepsilon_p) = \frac{U^2}{(2\pi)^2} \int \frac{(1 - f_{p-q})(1 - f_{k+q})}{\omega + \varepsilon_p - \varepsilon_{p-q} - \varepsilon_{k+q} - i\delta} d^2q. \tag{3}$$

There is a similar function, $\Pi^{(h)}$, in the hole–hole channel. The Fermi functions in the numerator define allowed regions of q space. For a given ω the integrand is singular along lines in q space which contribute to the imaginary part only when they intersect these regions. If we define

$$D(k, p, q, \omega) = \omega + \varepsilon_p - \varepsilon_{p-q} - \varepsilon_{k+q} \tag{4}$$

then the imaginary part of (3) can be written as a line integral

$$\operatorname{Im} \Pi^{(p)}(k, p, \omega) = \frac{U^2}{(2\pi)^2} \int \frac{f_p(1 - f_{p-q})(1 - f_{k+q})}{|\nabla_q D(k, p, q, \omega)|} dL_q \tag{5}$$

where dL_q is a line element along a contour of singularity in q space for a given frequency. The integral is performed over the first Brillouin zone which is a square. The square is divided up into N smaller elemental squares, each of which in turn is divided into two triangles with a bisecting diagonal that is parallel to the Fermi surface in each quadrant of the zone. In each triangle the denominator, D, is approximated by a linear function of q and the contribution of each triangle to the q integral can be written down exactly. The result for each triangle is summed to give the total q integral. This is done for a range of energy wider than the bandwidth. The second required momentum integration over p is done by a straightforward summation of the q-space results. This method of integration has been well tested in many contexts and is known to be numerically stable and convergent as the triangles get smaller. Using this technique we have been able to accurately evaluate the imaginary part of the second-order self-energy as a function of frequency for any point in k space.

There are other numerical calculations of self-energies in the Hubbard model. Many papers, though of interest, are concerned with the three-dimensional Hubbard model, such as the work of Treglia and co-workers [9], Taranko and co-workers [10] (who both discuss correlation effects in nickel) and Bulk and Jelitto [11], whereas we are concentrating exclusively on the two- and one-dimensional cases. Also, these authors use the 'local

approximation', i.e. a k-independent self-energy for which there is no sound justification in low-dimensional cases. Schonhammer and Gunnarsson [12] have also performed a similar self-energy calculation in the two-dimensional Hubbard model using density functional theory. Galan and Verges [13] have recently calculated a number of properties of the two-dimensional weak-coupling Hubbard model using a Lanczos diagonalization method on 4×4 lattices demonstrating the utility of the perturbative method for the Hubbard model.

The numerical technique described in this paper has not been used before in the evaluation of second-order self-energies in the Hubbard model. Schweitzer and Czycholl [14] have used a $1/N$ dimensional-expansion technique to calculate similar results. Our results for the self-energies are in close agreement with theirs, though they did not attempt a ladder-diagram calculation. The structure present in their self-energies is not discussed. In this paper it is possible to understand the origin of features present in the self-energies in terms of contributions to the integrals from disjoint regions of phase space, as discussed in section 4. This gives us confidence that the numerical method is sound and that the physical implications of self-energies of this sort in the ARPES experiments are plausible.

3. Results for half-filling

The first point of interest is to see if the application of the numerical method to the half-filled perfectly nested case corroborates the results of the analytic calculation of Virosztek and Ruvalds. Following their analysis we model the Cu–O plane using a square lattice. We use a two-dimensional tight-binding band of the form

$$\varepsilon_k = -\cos k_x - \cos k_y. \tag{6}$$

This gives a bandwidth, W, of 4 and we examine the second-order self-energy correction relative to a half-filled paramagnetic ground state: $n_{i\uparrow} = n_{i\downarrow} = 1/2$.

States are occupied up to $\varepsilon_k = 0$ where $|k_x| + |k_y| = \pi$ and are otherwise unoccupied. The first Brillouin zone is a square.

The imaginary part of the self-energy is calculated at points with $k = (1, 1)k/\sqrt{2}$ where (i) $k = k_f$, (ii) $k = 1.15k_f$, (ii) $k = 1.3k_f$ or (iv) $k = 1.5k_f$.

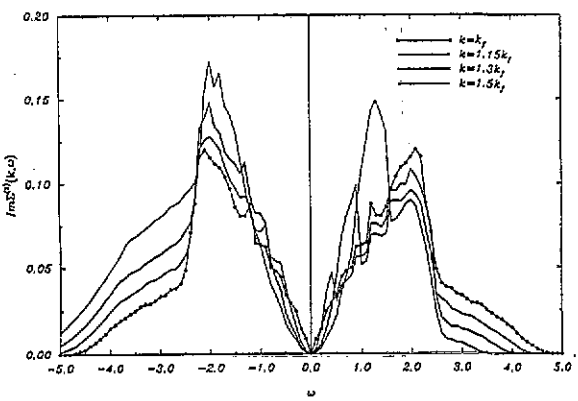

Figure 2. $\mathrm{Im}\,\Sigma^{(2)}(k, \omega)$ for four values of k along the (1, 1) direction in the half-filled case.

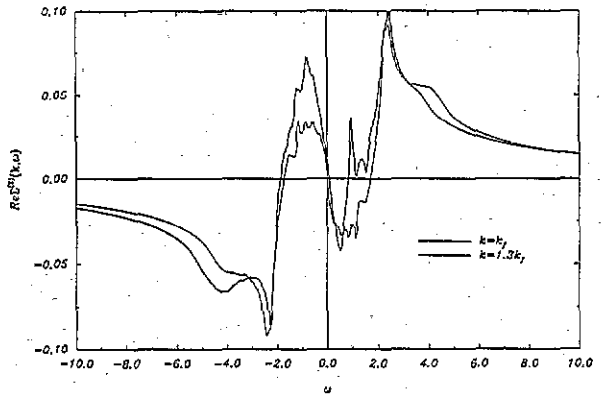

Figure 3. Re $\Sigma^{(2)}(k,\omega)$ for two values of k along the $(1,1)$ direction in the half-filled case.

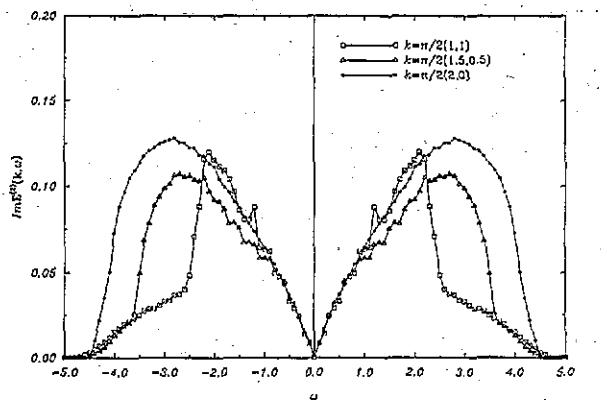

Figure 4. Im $\Sigma^{(2)}(k,\omega)$ for three values of k along the line $k_x+k_y=\pi$ in the half-filled case.

These four self-energies are shown in figure 2 and the corresponding real parts for $k=k_f$ and $k=1.3k_f$ are in figure 3. We have also calculated the imaginary parts of the self-energy at three other points and shown them in figure 4. At the zone corner the curve shows no significant structure, in contrast to the logarithmic singularity in the density of states at the saddle point. We therefore do not expect any significant breakdown in perturbation theory for the self-energy due to saddle-point effects.

To perform these calculations we divided the first Brillouin Zone into 6400 squares and found from the results that $\mathrm{Im}\,\Sigma^{(2)}(k,\omega)\propto\omega$ and $\mathrm{Re}\,\Sigma^{(2)}(k,\omega)\propto\omega\ln\omega$ for $k=k_f$ and low ω. In a conventional weak-coupling treatment of an interacting Fermi liquid at $T=0\,\mathrm{K}$ in two dimensions, $\mathrm{Im}\,\Sigma^{(2)}(k,\omega)\propto\omega^2\ln\omega$ [15]. Our numerical result agrees with the analytic calculation of Virosztek and Ruvalds and the marginal Fermi liquid hypothesis of Varma and co-workers. For k points off the Fermi surface the low-frequency linearity is lost and the usual non-linear behaviour is recovered. Our results show that linearity is only present for $k=k_f$ and is not maintained when k moves off k_f. This is in agreement with the calculations of Schweitzer and Czycholl [14].

The self-energies are plotted on a frequency scale of $W/40$ to ensure a reasonable resolution of structure. The choice of mesh size which is then used to perform the momentum integrals at each energy point is determined by the time taken to perform a calculation and the computer time available. In this case a mesh of 6400 squares was used, which typically took around fourteen hours to calculate the full frequency dependence of an imaginary self-energy at a given point in k space. The smaller irregularities in the imaginary self-energies are due to numerical effects whereas the structures described in the

next section are intrinsic, irrespective of the relative fineness of the momentum integration mesh.

4. Features of the self-energy calculations

The momentum dependence of the imaginary part of the self-energy when k moves off the Fermi surface shows interesting features that develop continuously as a function of k. A strong low-frequency peak with a nearly discontinuous upper edge emerges. This is clearly visible in figure 2. A corresponding structure also appears in the real part as a sinuosity which is visible in figure 3 near $\omega = 1$. For a quite moderate value of U/W this gives rise to an additional solution of the Dyson equation $\omega - \varepsilon_k - \mathrm{Re}\,\Sigma^{(2)}(k, \omega) = 0$. The emergence of this extra solution gives additional peaks in the calculated spectral weight and there is some experimental evidence for additional peaks in the ARPES results of Takahashi and co-workers [16] although other experiments do not show this [17]. In figure 5 we show a calculation of the spectral weight based on the second-order self-energies for $U/W = 3/4$ and at the point $\boldsymbol{k} = 0.7k_f(1, 1)/\sqrt{2}$. Takahashi interprets these ARPES features as arising from separate quasiparticle bands. Our results suggest that, if there, they arise from the additional solutions of the Dyson equation. It is not necessary to start off with a model involving two or more bands.

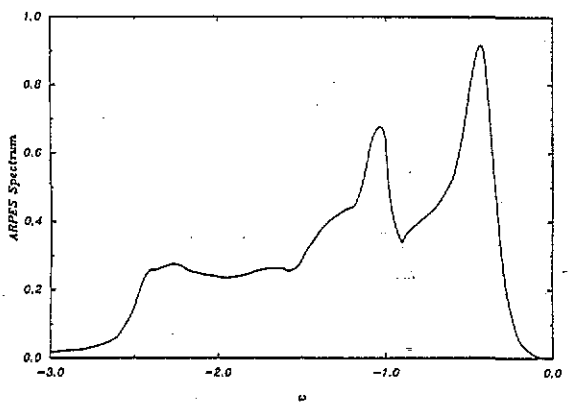

Figure 5. Calculated angle-resolved photoemission spectrum for $\boldsymbol{k} = 0.7k_f$ (1, 1) in arbitrary units. $U/W = 3/4$.

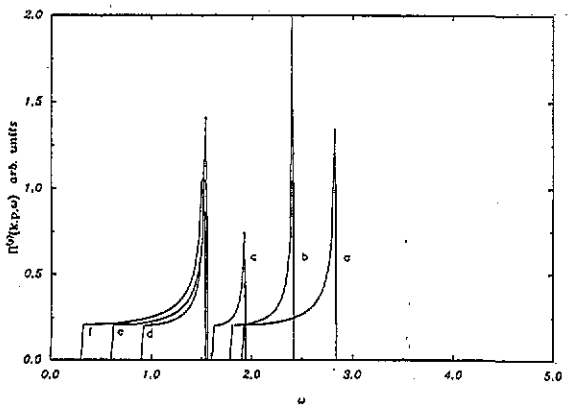

Figure 6. Vertex corrections, $\Pi^{(p)}$, for $\boldsymbol{k} = 1.5k_f$ (1, 1) and (*a*) $\boldsymbol{p} = 0.2p_f$ (1, 1), (*b*) $\boldsymbol{p} = 0.3p_f$ (1, 1), (*c*) $\boldsymbol{p} = 0.4p_f$ (1, 1), (*d*) $\boldsymbol{p} = 0.7p_f$ (1, 1), (*e*) $\boldsymbol{p} = 0.8p_f$ (1, 1), (*f*) $\boldsymbol{p} = 0.9p_f$ (1, 1).

It is important to understand the emergence of this peaked structure in the imaginary part of the self-energy and how it evolves with differing momenta. To do this we examine the individual contribution of each summation over q to the total self-energy integral by evaluating (3) for a selection of different p values. For convenience we will look at the imaginary part of the self-energy at $k = 1.5k_f(1,1)/\sqrt{2}$. In figure 6 the results of the q summations for six different p points are shown. There are three of these, labelled d, e and f, which have upper edges which coincide around the value $\omega = 1.5$ while the remainder, labelled a, b and c, have edges which disperse across a broad range of frequencies. The full result for $\mathrm{Im}\,\Sigma^{(2)}(k,\omega)$ is the sum of these and other contributions. The coincidence of the edges of many separate contributions gives rise to a strong peak in the imaginary part with a very nearly discontinuous upper edge. This effect depends on the way the Fermi factors in the numerator of (3) restrict the region of integration. There is also a bandstructure effect. To demonstrate this we consider points along the (1,1) direction so (4) can be written

$$D(k,p,q,\omega) = \omega - 2\cos(p) + 2\cos(k+q) + 2\cos(p-q). \tag{7}$$

To find the stationary points of this function we differentiate with respect to q and set the result to zero, i.e.

$$-\sin(k+q) + \sin(p-q) = 0 \tag{8}$$

so for a given k and p there are stationary points at

$$q = -\frac{k-p}{2} + n\pi. \tag{9}$$

For given k and p it is possible to calculate the energy of an edge in the q summation from

$$\omega = 2\cos(p) + 2\cos\left(k - \tfrac{1}{2}(k-p) + n\pi\right) + 2\cos\left(p + \tfrac{1}{2}(k-p) - n\pi\right). \tag{10}$$

In figure 7(*a*) we show the allowed region of q space for the p-value in figure 6 labelled (*a*). (In the two-dimensional Hubbard model the allowed region of integration is a hypervolume in a four-dimensional pq space, so we can only present two-dimensional slices through this space corresponding to fixed values of p.) Within the allowed region we show the contours on which the denominator in (3) is constant. As p increases further the allowed region over which the integrand exists shrinks until at some critical value of p it vanishes completely. The frequency of the upper edge of the q summation depends *strongly* on p up to the critical value as shown in figure 6(*a*)–(*c*).

As p increases beyond this critical value the allowed region reappears again, with the same shape, but displaced in q space by an amount $(+\pi, +\pi)$. A region is shown in figure 7(*b*). This corresponds to the q summation labelled (*d*) in figure 6. The width of the allowed region in q space grows as p increases from the critical value. Furthermore the frequency of the upper edge of the q summation now depends *weakly* on p as shown in figure 6(*d*)–(*f*). The overall result for the self-energy involves the summing of many such individual q summations from each p point. The q summations with edges at energies that are nearly coincident will, when summed, form the peaked structure visible in the imaginary part in figure 2. From (10) it is possible to see how the edges vary with energy in the two disjoint allowed regions and why in one region the edge dispersion is stronger than in the other. For graphs (*a*)–(*c*) in figure 6 we set $p = \pi/4 - \gamma$, $k = 1.5k_f = 3\pi/4$ and $n = 1$ and expand to get

$$\omega \simeq \sqrt{2} + 3.4\gamma. \tag{11}$$

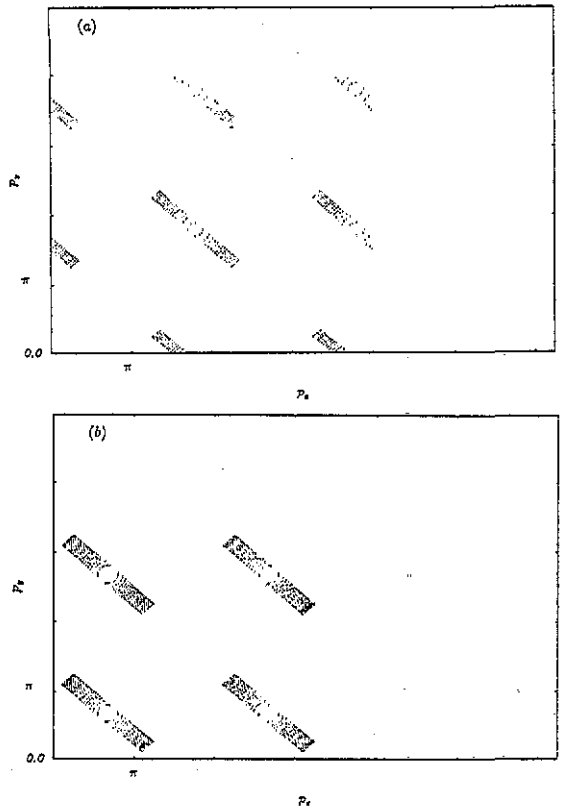

Figure 7. (*a*) Slice through allowed region of integration in q space when $p = 0.2p_f$ (1, 1). (*b*) Slice through allowed region of integration in q space when $p = 0.7p_f$ (1, 1).

For graphs (*d*)–(*f*) in figure 6 we set $p = \pi/4 + \gamma$ and $k = 1.5k_f = 3\pi/4$ and $n = 0$ and expand to get

$$\omega \simeq \sqrt{2} + 0.6\gamma. \tag{12}$$

From these two equations it is clear that in one region the position of the edge is strongly dependent on p whereas in the other this dependence is less strong so giving rise a very weakly dispersive edge energy in the q-summation results.

It is the splitting of the region of integration into two nearly disjoint regions that is the main characteristic of such self-energy calculations in two dimensions. When k is on the Fermi surface there is no splitting of the allowed region of integration so there is no low-energy peak. As soon as $k = k_f + \delta$, where δ is small but finite, a small piece of phase space is pinched off from the main region of integration which generates a small low-energy peak and a non-linear behaviour for $\omega \to 0$. For k values further from k_f the pinched off region grows thus pushing more weight into the low-energy peak. This development is clearly visible in the sequence of imaginary self-energies in figure 2.

In the case of the one-dimensional Hubbard model this splitting is easily understood and it shows up spectacularly in the appearance of strongly peaked structures at low frequencies. These structures have exactly the same physical origin as in the two-dimensional case and because of this have a small, but finite, width. As in the two-dimensional case, the integrity of the allowed region of integration for $k = k_f$ means there is no low-energy peak for this particular k value. In the one-dimensional case the allowed region of phase space is two-dimensional and a more explicit description of the region can be made. In figure 8 we show

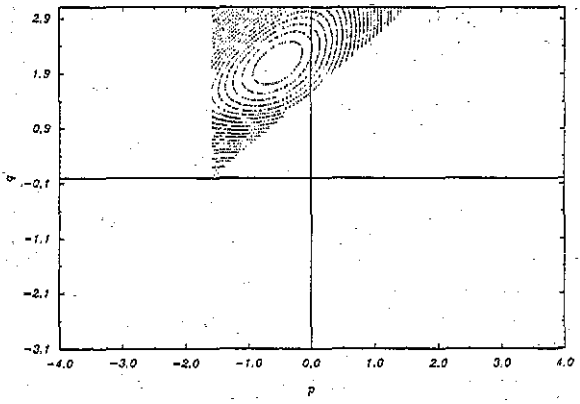

Figure 8. The whole of the allowed region of integration in pq space for the one-dimensional Hubbard self-energy, when $k = k_f$.

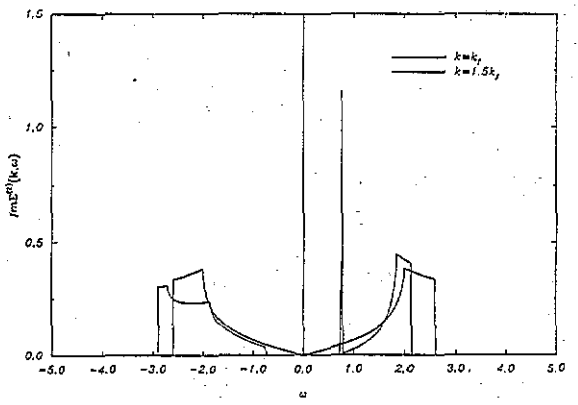

Figure 9. $\mathrm{Im}\,\Sigma^{(2)}(k,\omega)$ for the one-dimensional Hubbard model for two values of k.

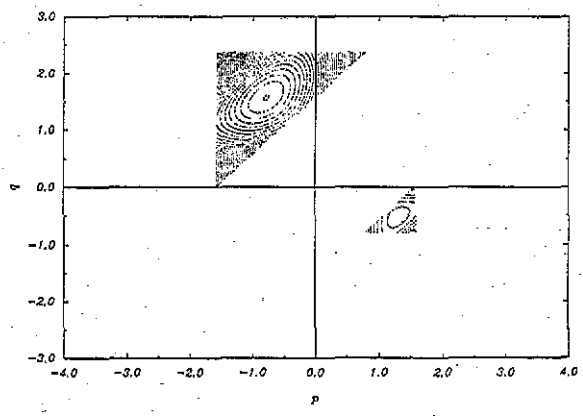

Figure 10. The whole of the allowed region of integration in pq space for the one-dimensional Hubbard self-energy, when $k = 1.5k_f$.

the allowed region of integration when $k = k_f$ and in figure 9 the corresponding imaginary part of the self-energy. This region is connected and hence there is no low-energy peaked structure in it. Also as $\omega \to 0$, $\mathrm{Im}\,\Sigma(k_f, \omega) \propto \omega$. For k off the Fermi surface the allowed region of integration shown in figure 10 is no longer connected, and a small disjoint region appears which gives rise to the strongly peaked low-energy structure visible in figure 9. This is directly analogous to the physical process giving rise to the peaks in the two-dimensional case. Some analytic results for this case have been produced by Zlatic and co-workers [22], which coincide with our numerical results in all respects. For the three-dimensional Hubbard

model such phenomena will be weaker because the characteristic van Hove singularities in three dimensions are weaker. In the next section we test the robustness of these features by using alternatives to the half-filled nearest-neighbour-hopping tight-binding scheme.

5. Away from perfect nesting

In section 4 the results for the imaginary part of the second-order self-energy were calculated with the tight-binding half-filled band of (6). A perfectly nested Fermi surface is perhaps a somewhat artificial representation of the electronic structure of the copper-oxide plane and may give rise to special effects that are lost at less than half-filling. We describe non-nested Fermi surfaces in terms of a doping parameter so that the Fermi surface is no longer flat, and include later next-nearest-neighbour hopping terms which have a similar effect.

From the same numerical method as before, we calculate the imaginary part of the second-order self-energy for the non-half-filled case. We use a bandfilling of 0.37. In figure 11 a sequence of four self-energies is shown for points along the (1,1) direction, starting on the Fermi surface and moving out towards the zone corner. Because perfect nesting is no longer present the linearity in the imaginary part at low frequencies is lost. Other calculations of $\mathrm{Im}\,\Sigma(k_f, \omega)$ at points on the Fermi surface also showed non-linear behaviour at low frequency. At much heavier doping levels, with no significant nesting, the low-frequency behaviour is definitely non-linear. However there are still strong low-frequency peaks up to a bandfilling of 0.31. An analysis of the allowed regions of momentum space in the doped case leads to conclusions similar to those in the perfectly nested case. Now the alteration of the shape of these regions due to doping changes the relative weights in the low-energy peaked structure only slightly. Because these peaks survive the loss of nesting our conclusions about the ARPES results are unchanged.

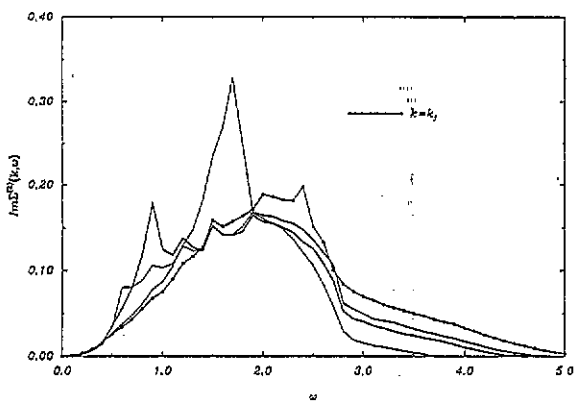

Figure 11. As for figure 2 but for a band filling of 0.37.

To include the effects of next-nearest-neighbour hopping term we put

$$\varepsilon_k - \mu = -\cos k_x - \cos k_y + A \cos k_x \cos k_y \tag{13}$$

where A is the next-nearest-neighbour hopping integral. Bandstructures of this sort have been used to describe the Fermi surfaces observed in some high-T_c materials [18].

In figure 12 we present a sequence of imaginary self-energies with a half-filled band and $A = 0.3$. Although the Fermi surface is of a quite different shape to that in the

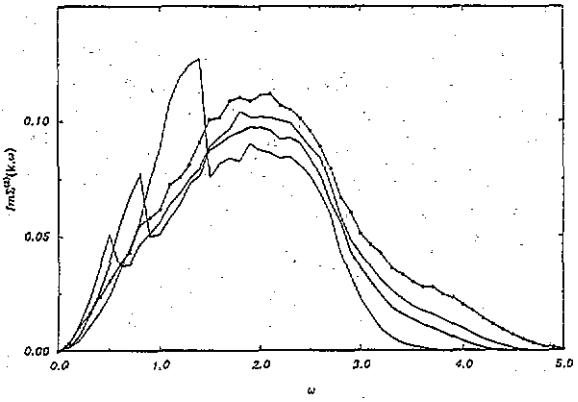

Figure 12. As for figure 2 but with next-nearest-neighbour hopping included; $A = 0.3$ and at half-filling.

perfectly nested case, strong peaks emerge in the low-frequency range indicating that this phenomenon is quite stable against considerable deformation of the Fermi surface.

The non-half-filled case with next-nearest-neighbour hopping included can also be considered. We chose $A = 0.2$ and a filling of 0.45. This a particularly special choice of Fermi surface because there are saddle-points in D where the Fermi surface meets the zone edge as in the perfectly nested band [19]. A sequence of imaginary self-energies along the $k = (1, 1)$ line is shown in figure 13. As before, a peaked structure is visible and evolves as k moves toward the zone corner.

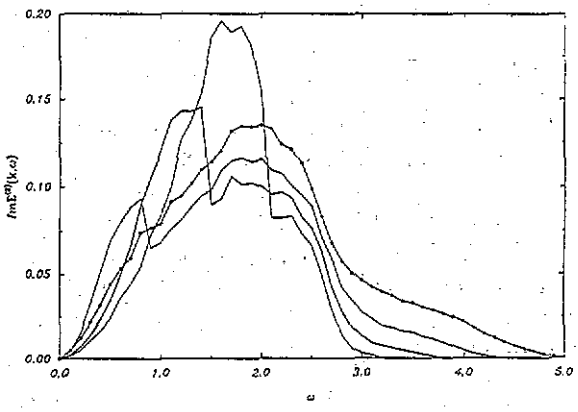

Figure 13. As for figure 2 but with next-nearest-neighbour hopping included; $A = 0.2$ and with a band filling of 0.45.

6. Ladder diagrams

In this section we will demonstrate the robustness of our new structure in the self-energy by showing that the simplest higher-order perturbative corrections enhance rather than diminish the structure. These corrections are the infinite sum of ladder diagrams of which an example is illustrated in figure 14. Ladders are mostly used in low-density situations rather than the high-density situations of this paper. However, ladder approximations *do* take into account multiple-scattering and excluded-volume effects. We shall further demonstrate that in the two-dimensional Hubbard model there are anti-bound states in the particle–particle channel (and bound states in the hole–hole channel) for any value of the interaction parameter

U however small. This is a rather trivial consequence of the fact that the characteristic van Hove singularities in two dimensions are discontinuities. This is a controversial and important topic because Anderson [20] claims that these anti-bound states are responsible for a low-energy catastrophe (rather like the soft x-ray singularity) which is responsible for the anomalous normal state properties of the high-T_c materials. Engelbrecht and Randeria [21] argue that there is no such catastrophe in any order of perturbation theory and that the Anderson effect cannot explain the data. We shall comment on this.

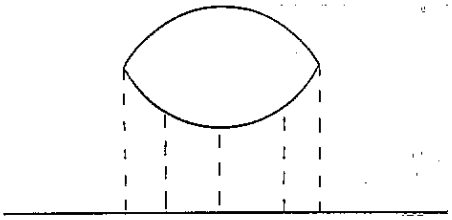

Figure 14. The self-energy diagram in the ladder calculation.

We sum the ladder diagrams of figure 14. The contribution to the self-energy from the particle–particle channel is

$$\Sigma^{(p)}(k, \omega) = 1/N \sum_{p} f_p \Gamma^{(p)}(k, p, \omega + \varepsilon_p) \tag{14}$$

where

$$\Gamma^{(p)}(k, p, \omega) = U[1 - U\Pi^{(p)}(k, p, \omega)]^{-1} \tag{15}$$

and $\Pi^{(p)}$ is defined in (3). There is a similar contribution from the hole–hole channel. In figure 15 we show Im $\Pi^{(p)}$ and Im $\Gamma^{(p)}$ for $p = 0.4\pi(1, 1)$, and $k = 0.75\pi(1, 1)$. We have used a small additional broadening to make the anti-bound state in $\Gamma^{(p)}$ clearly visible. In figure 16 we show Im $\Sigma^{(p)}$ for $k = 0.75\pi(1, 1)$ in second-order perturbation theory *and* in the ladder approximation for a bandfilling of 0.37. The anti-bound state arising from those contributions to $\Sigma^{(2)}$ which produce the low-energy bump are all at very nearly the same energy and can be clearly seen as a sharp peak in $\Sigma^{(p)}$. The width of this peak is mostly due to the artificial broadening which makes it visible. Because of the narrow width of this peak the *lifetime*, τ, of states in the peak is *long*.

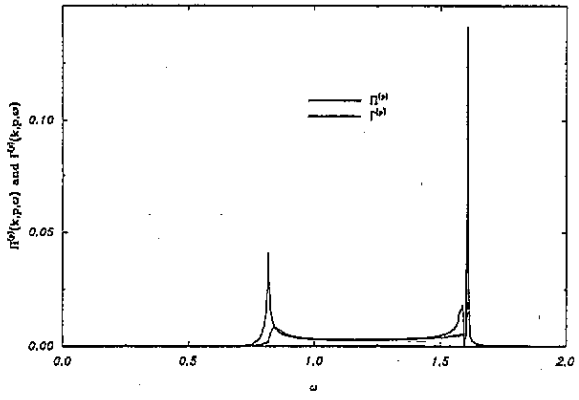

Figure 15. Vertex correction in second-order perturbation theory, $\Pi^{(p)}$, and in the ladder approximation, $\Gamma^{(p)}$ in arbitrary units.

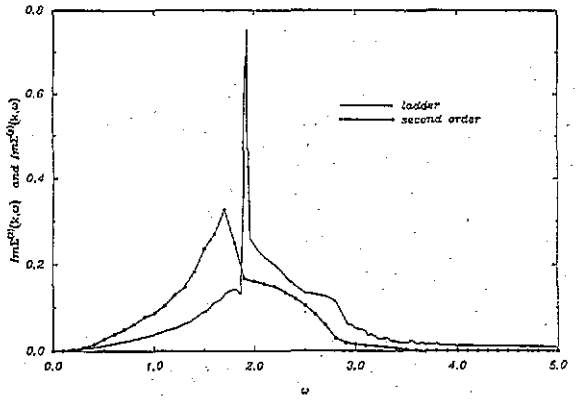

Figure 16. A typical result for $\mathrm{Im}\,\Sigma^{(p)}(k,\omega)$ in the ladder approximation showing the strong narrow peak at rather low frequencies due to anti-bound states and also the corresponding second-order self-energy $\mathrm{Im}\,\Sigma^{(2)}(k,\omega)$ for $k = 0.75\pi(1,1)$ and a bandfilling of 0.37. The result for the ladder calculation has been smoothed on the scale of the energy interval between successive points to remove numerical noise of known origin.

In the soft x-ray problem the scattering centre is a well-localized deep level on one atom in the system which has a long lifetime. It is important for the appearance of the low-energy catastrophe that this lifetime should be long compared to the time interval τ' over which the scattering event occurs. The results of the previous paragraph show that there is a good chance that $\tau' \ll \tau$ and that a low-energy catastrophe is possible in the Hubbard problem.

The energy of the peak, of course, changes as k changes but it remains of narrow width so that at a fixed value of k the low-energy catastrophe in $\Sigma(k,\omega)$ is possible. It is to this catastrophe that Anderson attributes the normal-state properties.

Perturbation calculations even of infinite order do not affect Anderson's argument because the soft x-ray singularity (or low-energy catastrophe) is an intrinsically non-perturbative effect.

7. Conclusions

In this paper we have investigated self-energies in the two-dimensional Hubbard model using a variety of bandstructures and band fillings. From our results we conclude that the linearity of the low-energy region of $\mathrm{Im}\,\Sigma^{(2)}(k,\omega)$ in the two-dimensional Hubbard model occurs only in perfectly nested bandstructures. Any deviation from perfect nesting is sufficient to destroy agreement with the marginal Fermi liquid hypothesis.

Our numerical methods enable us to investigate the momentum dependence of the self-energy. This shows the existence of strong low-energy peaks in the imaginary part which evolve continuously as k moves off the Fermi surface. We have shown that these structures arise from a splitting of the allowed region of integration into two disjoint regions and have illustrated this by examining the same process in the one-dimensional case. These strongly peaked structures, which also occur for non-nested Fermi surfaces, may have implications for ARPES measurements, though this has yet to be conclusively demonstrated.

We have evaluated the vertex function $\Gamma^{(p)}$ and the self-energy $\Sigma^{(p)}$ in the infinite-order ladder approximation and found anti-bound states pushed to higher energies in the particle–particle channel. From an analysis of the structure in the imaginary part of the self-energy we find evidence to support the view that the scattering in the two-dimensional Fermi system is analogous to that found in the soft x-ray problem.

Acknowledgments

Financial support for the work of CJR from an SERC Research Studentship is acknowledged. Helpful conversations with Professor D M Edwards, Dr Y Chen and Dr V Zlatic are also acknowledged.

References

[1] Lieb E H and Wu F Y 1968 *Phys. Rev. Lett.* **20** 1445
[2] Metzner W and Vollhardt D 1989 *Phys. Rev. Lett.* **62** 324
[3] Moreo A, Scalapino D J, Sugar R L, White S R and N E Bickers 1990 *Phys. Rev.* B **41** 2313
[4] Levin K, Kim J H, Lu J P and Si Q 1991 *Physica* C **175** 449
[5] Anderson P W 1987 *Science* **235** 1196
[6] Varma C M, Littlewood P B, Schmitt-Rink S, Abrahams E and Ruckenstein A E 1989 *Phys. Rev. Lett.* **63** 1996
[7] Virosztek A and Ruvalds J 1990 *Phys. Rev.* B **42** 4064
[8] Gilat G and Raubenheimer L J 1966 *Phys. Rev.* **144** 391
[9] Treglia G, Ducastelle F and Spanjaard D 1980 *Phys. Rev.* B **21** 3729
[10] Taranko R, Taranko E and Malek J 1989 *J. Phys.: Condens. Matter* **1** 2935
[11] Bulk G and Jelitto R J 1990 *Phys. Rev.* B **41** 413
[12] Schonhammer K and Gunnarsson O 1988 *Phys. Rev.* B **37** 3128
[13] Galan J and Verges J A 1991 *Phys. Rev.* B **44** 10093
[14] Schweitzer H and Czycholl G 1991 *Z. Phys.* **83** 93
[15] Luttinger J M 1960 *Phys. Rev.* **119** 1153
Hodges C, Smith H and Wilkins J W 1971 *Phys. Rev.* B **4** 302
[16] Takahashi T, Matsuyama H, Katayama-Yoshida H, Okabe Y, Hosoya S, Seki K, Fujimoto H, Sato M and Inokuchi H 1989 *Phys. Rev.* B **39** 6636
[17] Olsen C G, Liu R, Lynch D W, List R S, Arko A J, Veal B W, Chang Y C, Jiang P Z and Paulikas A P 1990 *Phys. Rev.* B **42** 381
[18] Yu J and Freeman A 1991 *J. Phys. Chem. Solids* **52** 11/12
[19] Newns D M, Tsuei C C, Pattnaik P C and Kane C L 1992 *Comments Cond. Mat. Phys* **15** 273
[20] Anderson P W 1990 *Phys. Rev. Lett.* **64** 1839; **65** 2306
[21] Engelbrecht J R and Randeria M 1992 *Phys. Rev.* B **45** 12419
[22] Zlatic V, Horvatic B, Schlieker G and Schotte K D 1992 *Phil. Mag.* B **65** 1255